Journal of Applied Physics PERSPECTIVE scitation.org/journal/jap

Perspective on photovoltaic optical power converters

Cite as: J. Appl. Phys. **130**, 160901 (2021); doi: 10.1063/5.0070860
Submitted: 9 September 2021 · Accepted: 5 October 2021 ·
Published Online: 27 October 2021

View Online Export Citation CrossMark

Simon Fafard[a] and Denis P. Masson

AFFILIATIONS

Broadcom, IFPD (Canada), Ottawa, Ontario K1A 0R6, Canada

[a]**Author to whom correspondence should be addressed:** simon.fafard@broadcom.com

ABSTRACT

Optical wireless power transmission (OWPT) can be used for applications that cannot access traditional power using metal wires. Photovoltaic power-converting III-V semiconductor devices are the core components required for achieving such remote and galvanically isolated power deployments. The development of high-efficiency power converters has already propelled several sensors and probe applications. This growing applied physics field is leveraging the use of ubiquitous laser diode products, now commonly available at various wavelengths. Novel multijunction designs, based on the vertical epitaxial heterostructure architecture devices, have recently allowed fiber-based and free-space applications to quickly progress to higher electrical powers and to benefit from other laser wavelengths. Here, we discuss the perspectives of such multijunction power converters from the viewpoint of realizing additional OWPT deployments and for enabling more probe, sensor, or electronic subsystem power capabilities. The Perspective hence provides a roadmap for devices achieving not only higher conversion efficiency, but also elaborates on the practical aspects necessary to concurrently push the power converters to higher output powers. The photovoltaic multijunction power-converting device is particularly a game-changer for smartly increasing the output voltage and therefore maintaining practical optimal external loads at high laser input powers. Examples of conversion efficiencies above 60% for output powers up to 17.5 W are demonstrated at ~808 nm in this study, and up to 22 W of output power is obtained with an efficiency of 48.9% at ~980 nm.

I. INTRODUCTION

In the past few decades, photovoltaic devices have been developed to convert not only sunlight but also laser power.[1–42] These Optical Power Converters (OPCs), often also called Laser Power Converters (LPCs), have been used for power links and radio-over-fiber,[43,44] long-distance and safe laser power beaming,[45] power electronics, and other applications.[46,47] The research activities in the field of power converters, and related photovoltaic devices, continue to grow and to suggest exciting future device improvements.[48–61] The physics of multijunction power converter devices is particularly interesting with unique phenomena such as strong luminescence coupling and recycling.[62–65]

We have previously shown[37] that multijunction OPCs with output powers below 1 W (often designated as "regular power") can be tailored to output voltages ranging from 4 to 30 V with conversion efficiencies up to >60%. Broadcom has introduced the 4 and 6 V devices as released products. Furthermore, the devices are now offered in the form-factor of "medium-power" (optical input power, $P_{in} < 6$ W) and "high-power" ($P_{in} < 50$ W). Multijunction OPC devices are quickly taking over their single-junction predecessors in power transmission applications requiring total galvanic and EMI (electromagnetic interference) isolation. The advancements achieved with the multijunction power-converting devices are expected to foster the deployment of power-over-fiber applications at different wavelengths. In this work, we discuss the perspectives of power-converting devices from the viewpoint of the device performance and of the key aspects that will lead to realizing additional OWPT deployments in the future. The study provides a brief overview of the status of the field. In addition, we present our new OPC device development results. We assert that the three key aspects that are guiding the roadmap for increased device deployments are (1) the wavelength of operation, (2) the available output power, and (3) the OPC efficiency. These three aspects are reviewed in detail in Secs. II and III. Various technological and physical

constraints on these aspects are reviewed, as well as the interplay between them.

II. BRIEF OVERVIEW

III-V semiconductors are recognized for their superior performance for photovoltaic devices.[61] This study focuses entirely on III-V devices and excludes discussions on other types of photovoltaic materials such as Si, II-VI, chalcopyrites, perovskites, and organics.

To better conceptualize the OWPT field, it is very useful to survey the various applications and also to review the OPC device capabilities. For that purpose, we introduce Figs. 1 and 2. Figure 1 illustrates the various OWPT applications; it is organized according to the OPC's output power and the wavelength of operation. Figure 2 is a *power converter performance chart* built from the results published in the literature. Figure 2 shows the OPC's two most important performance aspects. While much emphasis in the literature is given to the OPC's conversion efficiency, the OPC's output power capability is of prime concern for practical applications. Figures 1 and 2 are in many aspects intertwined due to the underlying historical and technical considerations. These aspects are discussed in more detail in the following paragraphs.

As deduced from Fig. 2, historically, many studies have been performed on GaAs single-junction OPCs (blue circles). Given the 1.42 eV bandgap of GaAs, many of the initial OWPT applications were engineered in the 800–850 nm range. Therefore, as shown in Fig. 1, OWPT applications for sensors and probes mostly expanded in the 800–850 nm range initially. Evidently, from Fig. 2, it is also clear that a large majority of the OPC output power results are in practice in the regular-power category. Concurrently, from the laser source perspective, the commercial aspects, the reliability, and the technical attributes of the available laser diode products often predominantly guide the selection of the optical input wavelength. Another key consideration is the laser light attenuation in the propagation medium of interest (e.g., fiber or air), which depends on the input wavelength selected.

The 808 nm laser diodes have been commonly available commercially, but the 980 nm laser diodes have also matured to an even more favorable status of reliability and cost ($/W).[66] This laser trend has expanded the sensor and probe OPC applications to longer wavelengths in the 980 nm range as illustrated in Fig. 1. The OPC results for the ~980 nm wavelengths are displayed as the purple data points on the power converter performance chart of Fig. 2. Compared to the 808 nm lasers, the 980 nm laser diodes nowadays typically feature higher output power capabilities. Therefore, the OWPT applications can benefit from expanding into the medium-power and the high-power classes, as illustrated in Fig. 1, especially in the 980 nm wavelength range. As the available output power increases to the medium-power range, active sensors, small electronics, power electronics, and communication links become viable OWPT applications. In the high-power range, power electronics isolated/remote/backup power supplies also become possible applications.

From the OPC device perspective, the increased input laser power has the effect of increasing the OPC output current (I_{mpp}) at an almost constant output voltage (V_{mpp}). The OPC's optimal load (R_{mpp}) is determined using the relation $R_{mpp} = V_{mpp}/I_{mpp}$, and it corresponds to the external load for which the OPC device will operate at its maximum power point and therefore at its highest efficiency. For single-junction OPCs, the unavoidable detrimental consequence is that the optimal load R_{mpp} eventually collapses to unpractically small values (few hundreds of milliohms). Evidently, from Fig. 2, it is also clear that the higher output powers are in practice only realized using multijunction OPC devices (data points with the "*Broadcom's VEHSA*" labels).

To that effect, Fig. 3 shows the earlier results demonstrating vertical multijunction OPC devices. Figure 3(a) depicts the schematic of the vertical epitaxial heterostructure architecture (VEHSA) structure. Figure 3(b) shows the results measured with the number of subcells ranging between 4 (PT4) and 20 (PT20), where PT*N* stands for a phototransducer multijunction device with *N* subcells.[56] The measured data demonstrated that peak conversion efficiencies with Eff > 60% can be obtained in all cases for GaAs OPCs designed in the 800–850 nm range.[12]

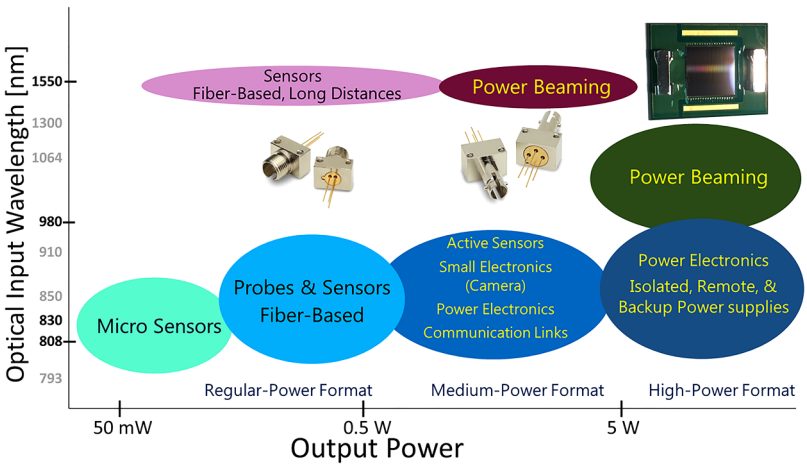

FIG. 1. Illustration of the various OWPT applications organized according to the OPC's output power (horizontal axis—log scale) and the wavelength of operation (vertical axis—not to scale). The commercial aspects, the reliability, and the technical attributes of the available laser diode products often predominantly guide the selection of the optical input wavelength. We classify the OPC devices into regular/medium/high power, based on their output power capabilities. Pictures of the corresponding Broadcom products are shown accordingly.

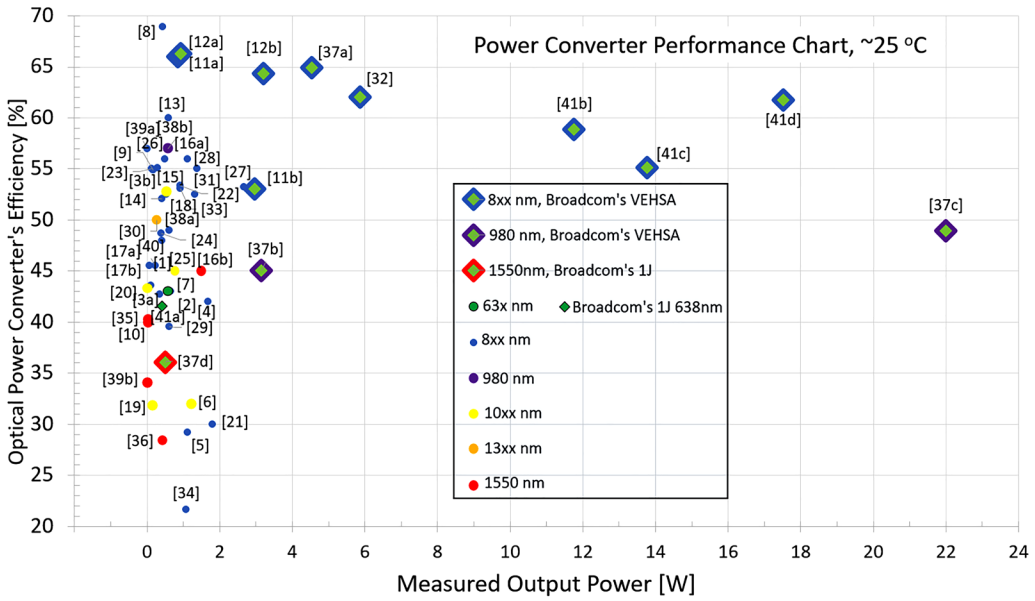

FIG. 2. Survey of the measured performance for monolithic power converter devices at the laser wavelengths indicated. Single junction, vertical multijunction, and planar segmented ("pizza" configuration) device reports are included (module results are not included here). [1] 1J-GaAs (2018) Jomen *et al.*,[1] [2] 1J-InGaP (2021) Komuro *et al.*,[2] [3a] Pizza-6 (2009) Schubert *et al.*,[3] [3b] Pizza-4 (2009) Schubert *et al.*,[3] [4] 6J-GaAs (2016) Zhao *et al.*,[4] [5] 6J-GaAs (2017) Sun *et al.*,[5] [6] 3J-InGaAsP (2020) Yin *et al.*,[6] [7] 4J (2018) Huang *et al.*,[7] [8] Back Mirror (2021) Helmers *et al.*,[8] [9] 1J-GaAs (2008) Oliva *et al.*,[9] [10] 1J-InGaAs (2013) Mukherjee *et al.*,[10] [11a] PT5 (2016) Fafard *et al.*,[11] [11b] PT12/8/6 (2016) Fafard *et al.*,[11] [12a] PT5 (2016) Fafard *et al.*,[12] [12b] PT12/20 (2016) Fafard *et al.*,[12] [13] 1J-GaAs (2016) Kalyuzhnyy *et al.*,[13] [14] 1J-GaAs (1992) Olsen *et al.*,[14] [15] 2J-GaAs (2007) Krut *et al.*,[15] [16a] 1J-GaAs (2003) Andreev *et al.*,[16] [16b] 1J-GaSb (2003) Andreev *et al.*,[16] [17a] Pizza-4 (2003) Peña *et al.*,[17] [17b] Pizza-6 (2003) Peña *et al.*,[17] [18] InGaAs (2020) Kalyuzhnyy *et al.*,[18] [19] InGaAs-Meta (2019) Kim *et al.*,[19] [20] 1J-InGaAsP (1981) Law *et al.*,[20] [21] 1J-GaAs (2019) Panchak *et al.*,[21] [22] Pizza-6 (2008) Bett *et al.*,[22] [23] Pizza-6 (1996) Fahrenbruch *et al.*,[23] [24] 1J-GaAs (1996) Fave *et al.*,[24] [25] 1J-Si (1992) Green *et al.*,[25] [26] 1J-GaAs (2016) Höhn *et al.*,[26] [27] 1J-GaAs-R_{mpp} = 0.38 Ω, (2015) Shan *et al.*,[27] [28] 1J-GaAs (2018) Khvostikov *et al.*,[28] [29] 1J-GaAs (2017) Khvostikov *et al.*,[29] [30] 1J-InGaAsP (2020) Helmers *et al.*,[30] [31] 1J-GaAs (2019) Zhao *et al.*,[31] [32] PT6 (2017) York *et al.*,[32] [33] 6J-GaAs (2018) Huang *et al.*,[33] [34] 6J-GaAs in TO (2017) Ding *et al.*,[34] [35] 1J-InGaAs (2014) Jarvis *et al.*,[35] [36] 1J-GaSb (2019) Khvostikov *et al.*,[36] [37a] PT6-GaAs (2021) Fafard *et al.*,[37] [37b] PT6-InGaAs (2021) Fafard *et al.*,[37] [37c] PT6-InGaAs (2021) Fafard *et al.*,[37] [37d] 1J-InGaAs (2021) Fafard *et al.*,[37] [38a] 3J-GaAs (2021) Keller *et al.*,[38] [38b] 5J-InGaAs (2021) Keller *et al.*,[38] [39a] 1J-GaAs (1997) Wojtczuk *et al.*,[39] [39b] 1J-InGaAs (1997) Wojtczuk *et al.*,[39] [40] Pizza-4 (2010) Eggert *et al.*,[40] [41a] 1J-InGaP (2021) Fafard *et al.*,[41] [41b] PT12 (2021) Fafard *et al.*,[41] [41c] PT5 (2021) Fafard *et al.*,[41] [41d] PT6 (2021) Fafard *et al.*[41]

Such a VEHSA device design has been described previously.[55,56] It consists of a photovoltaic vertical multijunction structure specifically built for operation with a narrow-band source such as a powerful laser. It is designed with several thin photovoltaic semiconductor subcells interconnected with tunnel junctions [TJ*i* in Fig. 3(a)], epitaxially grown on top of each other in a single Metal Organic Chemical Vapor Deposition (MOCVD) run. The emitter layer is generally n-type and the base layer is then p-type (i.e., an n-on-p configuration to take advantage of the higher electron vs hole mobility). The total thickness of all the emitter and base layers from the different subcells is such that almost 100% of the impinging optical beam is absorbed. The optically thin subcells are consequently connected in series (vertically), each generating a comparable photocurrent to achieve a high overall efficiency. To realize the required photocurrent matching condition, the structure has increasing subcell thicknesses from the top subcell (thinnest) toward the bottom subcell (thickest). For the OPCs intended for operation with an optical input in the 800–830 nm spectral range, the OPCs are based on GaAs absorber layers for the emitters (Si doped) and the bases (Zn doped). The number of subcells, *N*, effectively multiplies the device output voltage by a factor *N* compared to its equivalent single-junction device. The photocurrent is necessarily divided by the same factor *N*.

The bandgap of the absorbing layers determines the absorption characteristics of the multijunction photovoltaic device. For its current–voltage characteristics, this novel multijunction architecture effectively behaves as semiconductor material with an effective bandgap tailored to be $N \times$ Eg, where Eg is the bandgap of the constituent subcells (for example, Eg = 1.42 eV for GaAs). This is best visualized by measuring the dark current–voltage (I–V curves) of the PT*N* diodes. Figure 4 compares such dark I–V curves measured for single-junction (PT1-GaAs), PT4, PT6, and PT30 VEHSA devices. In the reverse bias, the current suppression is impressive, for example, resulting in only ~1 μA of current at a −35 V bias, for chips with an area of 0.032 cm^2. In the forward bias, the PT*N* diodes have an effective bandgap of a diode with $N \times 1.42$ eV for GaAs. Noticeably also, the PT*N* diodes exhibit extremely low series resistance. For example, straight lines are measured on the semi-log

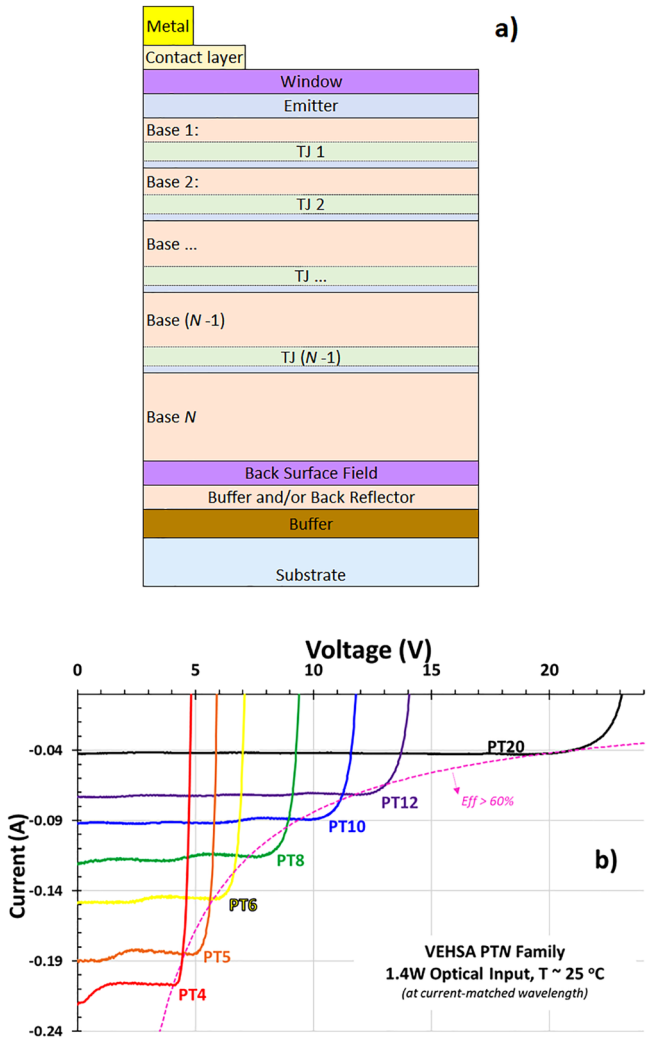

FIG. 3. Schematic in (a) and measured I–V curves in (b) of vertical epitaxial heterostructure architecture (VEHSA design) devices prepared with up to $N = 20$ p/n junctions. A spot near the central portion of a 3.7 × 3.7 mm^2 chip is illuminated and the resulting conversion efficiencies are between 60% and 66%. The optical input is set at current-matched wavelengths. Adapted from S. Fafard, F. Proulx, M. C. A. York, L. S. Richard, P. O. Provost, R. Arès, V. Aimez, and D. P. Masson, Appl. Phys. Lett. 109, 131107 (2016). Copyright 2016 Author(s), licensed under a Creative Commons Attribution (CC BY) license.[12]

plots, up to high forward bias currents. Indeed, the series resistance extracted from such dark I–V curves, or from the related illuminated I–V curves, is typically in the milliohms range.

For the device intended for operation with a laser in the 960–990 nm spectral range (e.g., purple diamond symbols in Fig. 2), the above GaAs absorbers are changed to InGaAs absorber layers with a band edge at about 1025 nm. For the 1500–1600 nm OPCs, InGaAs lattice-matched to InP is used for the absorber (e.g., red diamond symbols in Fig. 2).

Obtaining ~100% optical absorption of the laser input is attained in the VEHSA architecture by knowing the absorption coefficient and by distributing the necessary absorber thickness adequately in the different subcells. It is worth noting that achieving close to 100% absorption in single-junction devices can be more problematic. That is because single thick cells will have performance degradation when the minority carrier diffusion length becomes comparable to the cell thickness.

The measured external quantum efficiency (EQE) for the GaAs OPCs is around 94% at the peak of the spectral response.[11,12] The reflectivity from the anti-reflection coatings and the metallization is in the 2%–5% range, yielding high internal quantum efficiency (IQE) values. In addition, the vertical stacking design makes such OPC devices highly tolerant to beam non-uniformity, partial illumination, and beam misalignment.[47] The VEHSA devices are also tolerant to spectral variations of the laser input. Overall, the multijunction OPCs provide the best available conversion efficiencies for wide temperature ranges and cover the requirements for most OWPT applications. For example, Fig. 5 shows the performance of a group of over 3000 devices of the regular-power PT6 devices design for operation in the 800–830 nm spectral range (Broadcom's AFBR-POC206A1 product). The corresponding performance histograms for this group are presented in Fig. 6 for the measured EQE at 6.0 V in (a) and for the conversion efficiency in (b). As can be observed in Figs. 5 and 6, tight quasi-normal distributions are observed: the average values are EQE (6.0 V) ~ 89% and Eff (1.2 W at 828 nm) ~ 61.4%.

To analyze in more detail the OPC device behavior, the single diode equation can be adapted to model the behavior of the PT*N* VEHSA devices under illumination. For the PT6 of Fig. 5, we use six single GaAs diodes connected in series, all with the same bandgap of 1.42 eV. For simplicity, we assume that the six subcells have the same saturation current (J_o), ideality factor (n), and reverse bias breakdown characteristics. The optical input power is set to 1.2 W at 828 nm as per the experimental conditions, and the current matching between the various subcells is adjusted using an empirical factor. The resulting fit is shown in Fig. 5 as the dotted black curve. A good fit is obtained and the average efficiency of Eff = 61.4% is reproduced here using the following parameters: $n = 1.74$, $J_o = 7E\text{-}9$ mA/cm^2, series resistance = 0 Ω, current mismatch of 6.5% between the subcells with the highest and lowest currents. In this particular case, the optical input at 828 nm is at a wavelength longer than the peak of the spectral response. Therefore, the lower photocurrent is expected to be in the uppermost subcell and the higher photocurrent would be in the lowermost subcell. It is also noticeable that in the occurrence of current mismatch due to slight spectral detuning as in Fig. 5, the main kink in the I–V curves typically occurs around mid-voltage (here ~3.25 V). It is consistent with the upper half of the subcells being overdriven or starved with respect to the bottom half of the subcells, depending on if the optical input wavelength is, respectively, on the shorter or longer side of the peak of the spectral response. The other key parameters of interest are extracted as follows: the open circuit voltage, $V_{oc} = 7.232$ V; the voltage at the maximum power operating point, $V_{mpp} = 6.406$ V; the short-circuit current, $I_{sc} = 125.7$ mA; and the current at the maximum power operating point, $I_{mpp} = 155$ mA.

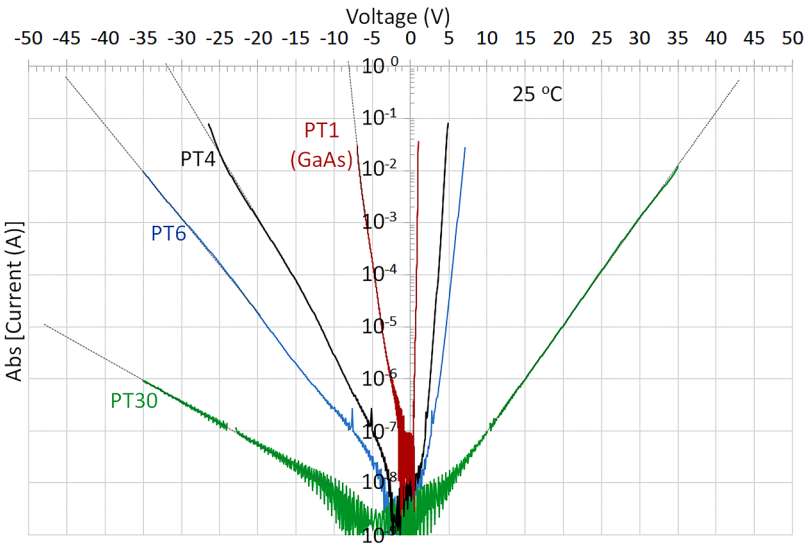

FIG. 4. Measured dark I–V curves for GaAs-based PT*N* VEHSA diodes, with $N = 1$ (single-junction GaAs), $N = 4$, $N = 6$, and $N = 30$, as indicated. The device area is here 0.032 cm^2.

An alternative approach to the vertical multijunction design is the planar multi-segment design (often also called the "pizza" configuration). Figure 2 shows the corresponding results obtained from various studies (e.g., data points [3a], [3b], [17a], [17b], [22], and [40]). In this approach, segments of single-junction devices are interconnected in a planar configuration with microfabrication processes. The multi-segment devices typically offer a wide spectral range of operation based on their single-junction design. However, they are particularly sensitive to beam misalignment and partial or non-uniform illumination. Furthermore, this pizza device design typically suffers from significant resistive losses due to the requirements of lateral current conduction within semiconductor layers. Still, interesting innovations have recently been proposed, including thin film designs with metalized back surfaces.[67,68] However, from the perspective of achieving a better path to simultaneously obtaining higher efficiencies and higher output power, the focus of this paper remains on the vertical multijunction OPCs.

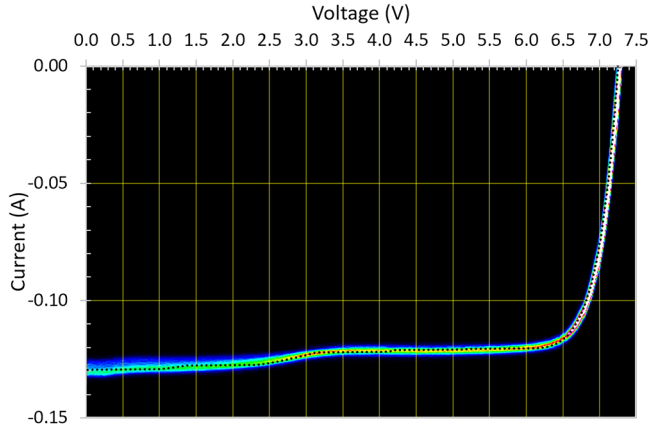

FIG. 5. Performance of regular power PT6 from a group of over 3000 devices (Broadcom's AFBR-POC206A1). Measured at room temperature ($T \sim 23$ °C) with an input power of 1.2 W at 828 nm. The density plot of all the current–voltage (I–V) curves is traced using a rainbow color scheme (cold colors correspond to lower occurrence points and hot colors correspond to higher occurrence points). The dotted black line on top of the density plot is a six-diode fit obtained using an adjusted ideal-diode model. Adapted from S. Fafard, D. Masson, J.-G. Werthen, J. Liu, T. C. Wu, C. Hundsberger, M. Schwarzfischer, G. Steinle, C. Gaertner, C. Piemonte, B. Luecke, J. Wittl, and M. Weigert, Energies 14(15), 4395 (2021). Copyright 2021 Author(s), licensed under a Creative Commons Attribution (CC BY) license.[37]

III. PERSPECTIVE

A. Perspective on higher output powers

As stated in Sec. I, we expect that the following three key aspects will be guiding the roadmap for future OWPT deployment growth:

(1) the wavelength of operation must be selected to piggyback on other industrial sectors that have already achieved laser diode products with high output powers, low $/W, high reliability, and good beam quality;
(2) the availability of higher OPC output powers will unlock new OWPT applications;
(3) the OPC's conversion efficiency must be maintained high to reduce the burden on the thermal management of the system.

Together, aspects (2) and (3) define the upper right quadrant of Fig. 2. For the wavelength selection, both the 808 and 980 nm laser diode products nowadays have remarkable output powers. Nevertheless, the 980 nm lasers tend to feature some of the best reliability for lasers with high output power. From a commercial perspective, the 980 nm diodes also already have among one of the best $/W parameters. Therefore, as shown in Fig. 1, 808 nm will remain an important spectral range, but ~980 nm is expected to

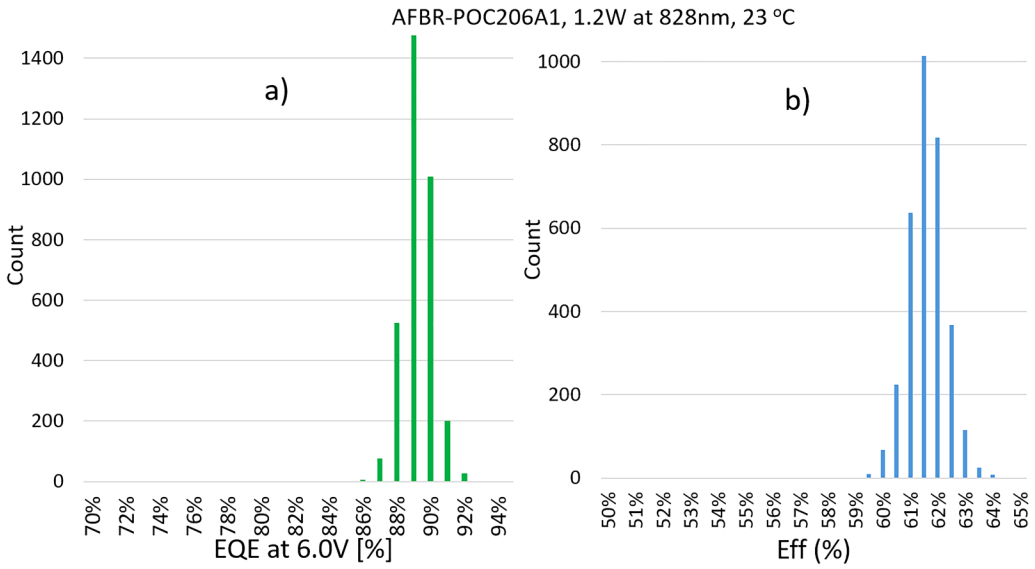

FIG. 6. Histograms of the performance of the group of over 3000 PT6 devices presented in the I–V curves of Fig. 5. EQE measured near the maximum power point at a voltage of 6.0 V in (a) and optical conversion efficiency in (b).

gain significant commercial traction as more OPC options become available in that spectral range.

To achieve higher OPC output powers while maintaining high efficiencies, it is necessary to increase the device output voltage. Otherwise, the optimal load collapses to unusable small values. The latter is also evidenced in Fig. 2, which shows that the single-junction reports can generally only rank in the regular power category. In practice, when the ratio of V_{mpp} over I_{mpp} becomes smaller than ~1 Ω, it becomes very problematic to maintain high conversion efficiencies. The high power capability of multijunction OPCs is further demonstrated in Fig. 7. The plots are showing the output characteristics and the optimal load for the medium-power PT6 OPCs (Broadcom's AFBR-POC306A1) in (a) and for the high-power PT12 OPCs (Broadcom's AFBR-POC512A1) in (b).

In both cases, record efficiencies are obtained for such unprecedented output power capabilities. With an output of $P_{mpp} = 4.54$ W, the PT6 has an efficiency of Eff = 64.9% for an optical input of ~808 nm. The open circuit voltage is $V_{oc} = 7.435$ V, which delivers a remarkable output voltage per subcell of 1.239 V. It corresponds to a particularly small bandgap voltage offset value of $W_{oc} = 0.181$ V, where $W_{oc} = (Eg/q) - V_{oc}$ with Eg being the bandgap energy (here of GaAs) and q is the electronic charge.

The high efficiency and output power capabilities of the medium power OPCs of Fig. 7(a) are predetermined from the higher output voltage characteristics of the PT6. Indeed, an optimal load of $R_{mpp} \sim 10\ \Omega$ is maintained at an output power of 4.54 W. It is worth noting that the optimal load for a PT6 compared to the corresponding GaAs single device is approximately 36× larger. That is because it runs at about 1/6 the output current and 6x the output voltage. The larger optimal load is very favorable and necessary for avoiding high output currents and the associated resistive losses, $I^2 \times R_{series}$, where R_{series} can be any external parasitic series resistance such as wiring, but also gridline and sheet conduction resistances from the carrier extraction within the chip itself. The PT12 of Fig. 7(b) features even higher output power capabilities because the optimal load is now roughly 144× larger compared to the corresponding GaAs single device. Here, over 13 W of output power is obtained.

The typical P_{out} vs P_{in} relationship of the high-power PT12 OPCs is shown in Fig. 8 (green square symbols). A slope efficiency of ~59% is measured with negligible deviations from a linear regression, here for optical input powers up to 20 W. The AFBR-POC512A1 device is designed to handle at least up to 50 W of input power, but the $/W limitations for the 808 nm lasers make it strategic to switch to 980 nm lasers for such high optical powers. For example, Fig. 8 also shows the measured P_{out} vs P_{in} relationship of the high-power PT6 OPCs designed for the 980 nm spectral range. For the latter, a somewhat lower slope efficiency is observed. In this case, the lower performance of the 980 nm OPC devices is at least in part attributable to the replacement of the GaAs with InGaAs for OPC's absorber material. However, we believe that subsequent iterations of the PT6-97x devices will result in comparable performances.

In any case, as demonstrated in Fig. 8, the availability of higher power laser diodes for the 980 nm spectral range typically more than compensate a slightly lower conversion efficiency for OPCs in that spectral range. In the case presented here, almost twice the output power is achieved for 980 nm OPCs, reaching an output power of $P_{mpp} \sim 22$ W. In the previous work, we have also demonstrated the reliability and stability of the VEHSA devices. For example, continuous stable ~22 W operation was performed for over 1000 h.[37]

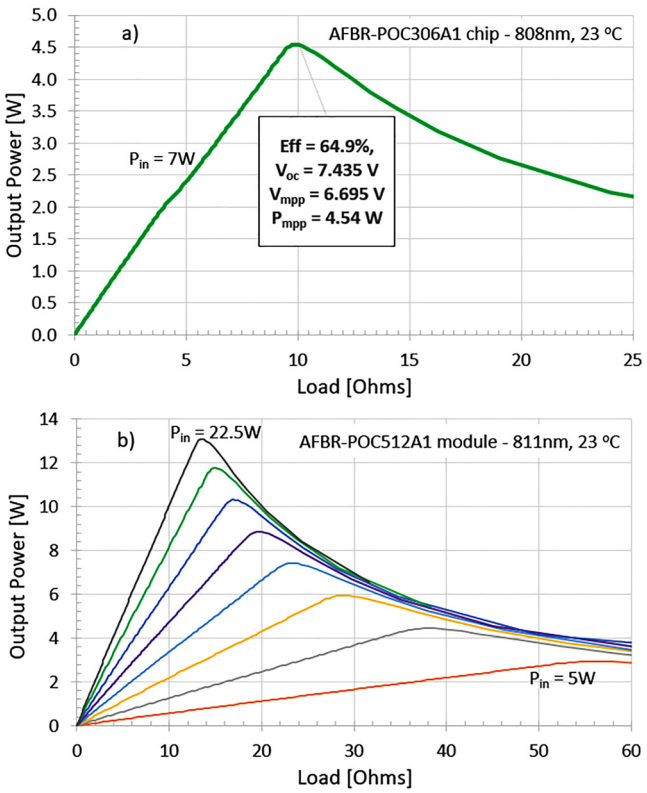

FIG. 7. Measured output power vs external load value for a typical medium-power PT6 chip (Broadcom's AFBR-POC306A1) in (a) and for a high-power PT12 device (Broadcom's AFBR-POC512A1) in (b). The optical input power is 7 W in (a) and varied from 5 to 22.5 W by increments of 2.5 W in (b). The chip area is 0.14 cm^2 for the medium-power device in (a), giving an average optical intensity of 48 W/cm^2. It is 1 cm^2 for the high-power device in (b), giving an average optical intensity of 22.5 W/cm^2 for the highest input power used here.

As illustrated in Figs. 1 and 2, the new range of combined high power and high efficiencies, enabled by the vertical multijunction VEHSA devices, can ignite new OWPT system capabilities and applications. These applications typically also require operation at various temperatures. In the previous work,[37] we have demonstrated that the VEHSA devices maintain good performance over the required operational ranges. To exemplify, Fig. 9 reproduces the measured temperature behavior for the PT6 and PT12 devices at 808 nm in (a) and for the PT6 devices at 980 nm in (b). Figure 9 shows output power capabilities in excess of 3 W at all temperatures for the 808 nm devices, and just slightly lower than 3 W for the 980 nm case. The measured conversion efficiency at 808 nm is reaching a maximum Eff > 64% for both the PT6 and the PT12.

B. Perspective on modules and arrays

All the results discussed above were obtained with monolithic discrete devices. In supplement, for OWPT applications requiring even more operational power, strings or arrays of devices can be

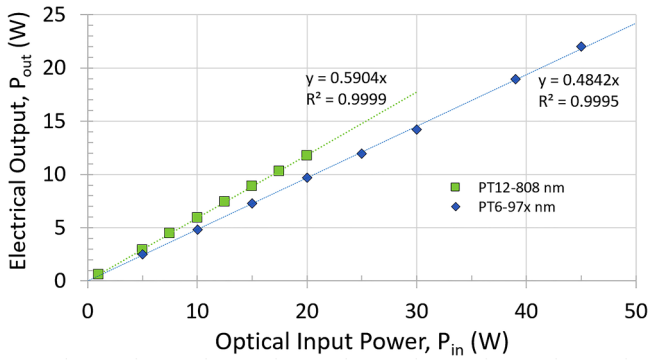

FIG. 8. Measured output power vs optical input power curves for the high-power PT12-808 nm OPCs (Broadcom's AFBR-POC512A1) with green square symbols and for the high-power PT6-97xnm OPCs (Broadcom's AFBR-POC506A5) with blue diamonds. The output power (i.e., $P_{out} = P_{mpp}$) vs P_{in} relationship is found to have negligible deviations from a linear regression, with the correlation factor and slope efficiencies as indicated. The chips are 1 cm^2 in size and maintained at ~23 °C.

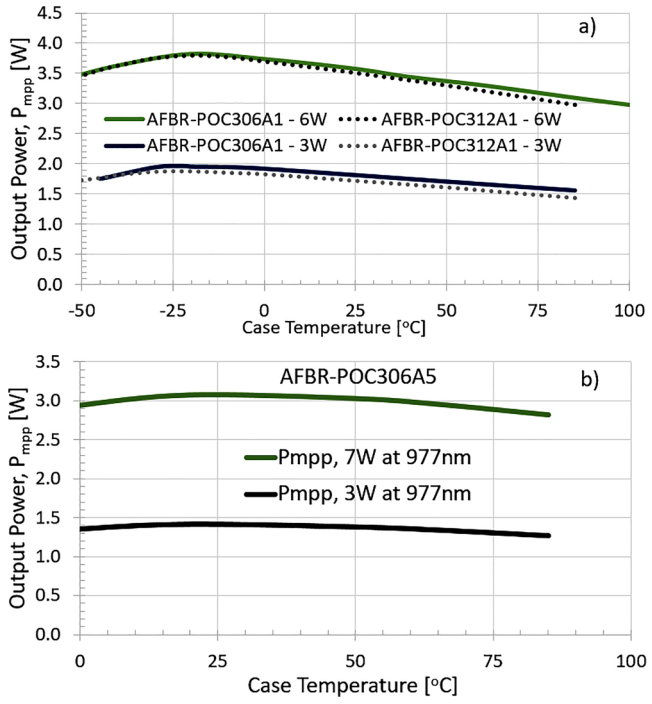

FIG. 9. Temperature dependence of the output power for medium-power OPCs for the spectral range of 800–830 nm in (a) and for 960–990 nm in (b). Test details are indicated on the plots. The average optical intensities are 20.8, 41.6, and 48.5 W/cm^2 for the P_{in} of 3, 6, and 7 W, respectively. Reproduced from S. Fafard, D. Masson, J.-G. Werthen, J. Liu, T. C. Wu, C. Hundsberger, M. Schwarzfischer, G. Steinle, C. Gaertner, C. Piemonte, B. Luecke, J. Wittl, and M. Weigert, Energies 14(15), 4395 (2021). Copyright 2021 Author(s), licensed under a Creative Commons Attribution (CC BY) license.[37]

used to deliver the required stable output.[37,69–72] For free-space beaming applications, dense arrays can be constructed. The optics of the beaming system needs to produce optical intensity profiles with good uniformity to maximize the efficiency of the system. For fiber-based applications, a number of discrete devices can be interconnected. For example, Fig. 10 shows the measured I–V curve obtained for a 3 × 4 array giving an output power of 44.9 W with a peak efficiency of Eff = 61.6%. This example is using three parallel strings of four medium-power PT6 connected in series, based on Broadcom's AFBR-POC306A1. Continuous stable operation of the 3 × 4 array has also been verified with an output power steady at >40 W for over 1000 h.[37]

The array can be used directly as a stand-alone power supply. It outputs ∼25 V near the optimal load, at 1.76 A. It outputs varying voltages if the load is changed, as per the I–V curve of Fig. 10. Alternatively, the array can be operated in conjunction with a regulating electronic DC-DC up/down converter. The latter approach allows obtaining a regulated output voltage with a set value. For example, Fig. 11 shows the results obtained using a readily available commercial down converter. Here, the selected DC-DC down converter had a measured conversion efficiency of ∼95.5% for an output power of 40 W at 16 V (output current of 2.5 A).

As indicated in Fig. 11, the regulated output was set to operate at voltage values between 12 and 20 V while using for its input source the 3 × 4 array of Fig. 10. The left vertical axis of Fig. 11 shows the measured output power when the output load was varied, here between ∼3.5 and 10 Ω. The measurements were performed for optical input powers on the 12 OPCs set at either 5 W (green curves) or 6 W (blue curves). Horizontal dashed lines indicate the points above where overall optical-to-electrical efficiencies better than 55% are achieved. The output powers of Fig. 11 include the conversion losses of the electronic DC-DC converter. The optimal load is reached when the OPC array is not able to provide enough power as an input source to the DC-DC converter. The corresponding operating OPC case temperatures were also measured and are shown on the right vertical axis of Fig. 11. As can be expected, when the load is tuned away from the optimal values, the OPC efficiency decreases and the excess optical power entering the OPCs is converted into heat. The excess heat then raises the OPC's operation temperatures, as shown in Fig. 11.

Proper thermal management of the OPC devices is indeed a key consideration and is the topic studied in more detail in Sec. III C.

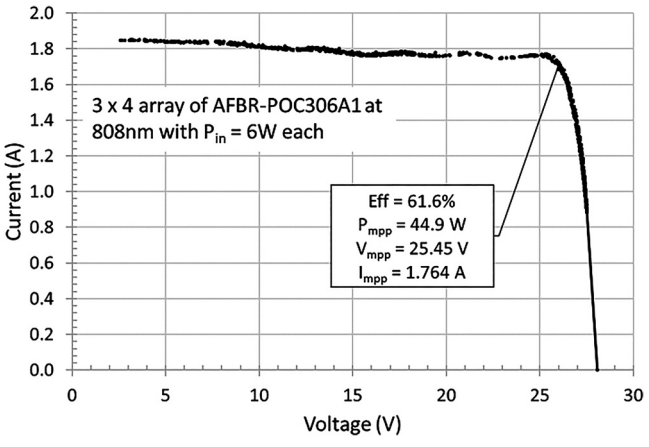

FIG. 10. Measured I–V curve at 23 °C for the 3 × 4 array of medium-power PT6 (Broadcom's AFBR-POC306A1) with 808 nm optical input.

C. Perspective on thermal management

It is essential to recall that all the optical input power impinging on an OPC device is either converted into valuable electrical power by the OPC or wasted into heat within the OPC's immediate thermal environment. In addition, unavoidably, the OPC's performance tends to decrease monotonically with increasing temperatures for the typical operating conditions. The medium-power PT6 and PT12 have been measured to maintain an efficiency of ∼50% for a case temperature of T_{case} ∼ 90 °C. Both the AFBR-POC306A1 and the AFBR-POC312A1 have a similar temperature coefficient of about −0.14%abs/°C.

It is important to optimize the thermal management strategy in order to maintain a high conversion efficiency and/or to avoid operating at excessively high device temperatures.[73] Thermal interface material (TIM) with a low thermal resistance must be used to adjunct the OPC device to its heatsink surface. In addition, the heatsink dimensions and material must be adequately engineered to handle all intended operation conditions. For that purpose, Fig. 12 shows examples of the measured thermal properties of regular-power and medium-power OPCs for various configurations. The results

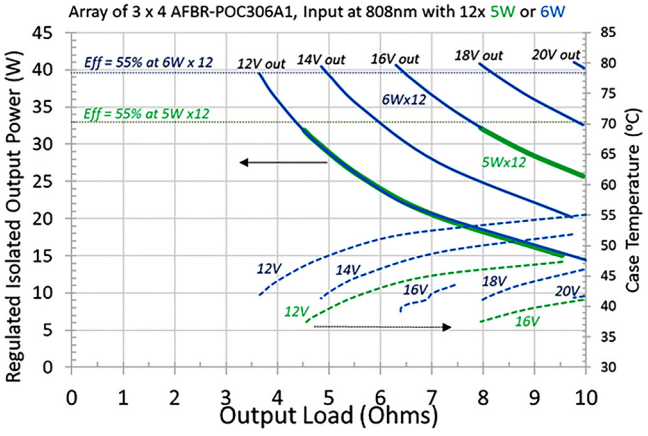

FIG. 11. Measured output performance for the voltage-regulated 3 × 4 array of medium-power PT6 (Broadcom's AFBR-POC306A1). Load dependence of the output power (left axis) and of the corresponding OPC case temperature (right axis) for different selected output voltages (12–20 V) and optical input powers (5 and 6 W at each OPC), as indicated. Steady-state operation with ambient at ∼23 °C. The operation with 16 V output with a 12 × 6 W optical input is reaching over a 55% optical-to-electrical efficiency and has been tested continuously for 1000 h of stable operation with an output of 40 W (an output current of 2.5 A).[37]

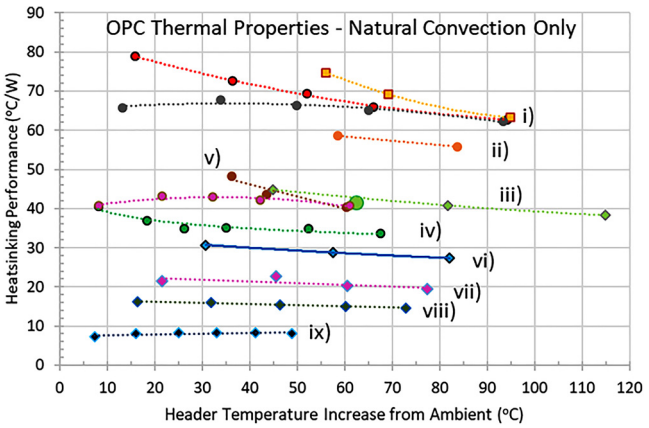

FIG. 12. Measured thermal properties of OPCs for various configurations: (i) Regular-Power no heatsink, (ii) Regular-Power on FR4, (iii) Medium-Power no heatsink, (iv) Regular-Power on 55 g plate, (v) Regular-Power with 3 g heatsink, (vi) Medium-Power with 3 g heatsink, (vii) Medium-Power with 17 g heatsink, (viii) Medium-Power with 29 g heatsink, and (ix) Medium-Power with 160 g heatsink.

presented in Fig. 12 are for heatsinking based on natural convection only, using aluminum for the heatsink material. If the OWPT application permits, air circulation can improve greatly the OPC's cooling. Air circulation can be achieved by using an externally powered fan or a fan self-powered from the OPC's output. The details of the optimization of the self-powered cooling system are beyond the scope of this study, but to exemplify the concept, about 0.2 W from the output of the high-power PT6-97x of Fig. 8 was diverted to drive a small fan in a voltage-limited regime for cooling the PT6-97x itself while the optical input power was kept at ∼45 W. Despite consuming 0.2 W for the fan, the overall available output power was significantly higher when using such a self-powered fan mode. For Fig. 12, we consider the situation of passive heatsinks without any air circulation. The standard-power and medium-power OPCs are themselves constructed predominantly from brass metal and have a weight of ∼6 and ∼11 g, respectively.

Figure 12 shows that the regular-power OPC without any heatsink is measured to have a thermal performance of about ∼65 °C/W, depending on the temperature increase from ambient (curve i). Mounting the OPC on a typical FR4 circuit board does not provide significant additional cooling (curve ii). Mounting the OPC on a metal frame (e.g., 55 g plate) improves the heatsinking performance to ∼35 °C/W (curve iv). Therefore, a regular-power OPC in an ambient of 25 °C running with an efficiency of 50% at an input power of 2 W would maintain a steady case temperature of ∼60 °C.

As another example from Fig. 12, the medium-power OPC with a 17 g heatsink has a heatsinking performance of ∼20 °C/W (curve vii). Therefore, a medium-power OPC in an ambient of 25 °C running with an efficiency of 50% at an input power of 6 W would maintain a steady case temperature of ∼85 °C.

Some OWPT applications may impose spatial restrictions that are limiting the heatsink selection to smaller dimensions. However, it is clearly advantageous to maximize the heatsink size whenever possible. It allows optimizing the system's heatsinking performance and maintaining higher OPC performance.

Another key consideration for OWPT applications is the selection of the spectral range. Section III D elaborates some key aspects for the OPC and laser wavelength selection.

D. Perspective on wavelength selection

Many intertwined factors influence the wavelength selection for OWPT applications. Fiber-based and free-space applications often have different considerations, especially as it related to eye-safety concerns,[74] the absorption within the propagation medium, and the laser beam properties. In this section, we will only focus on the spectral factors that can affect the OPC's performance.

The photovoltaic semiconductor material imposes a key trend from its fundamental responsivity characteristic: long wavelength photons have a higher photon flux for the same optical power. Indeed, the current (in Amps) from a PT*N* OPC device can be conveniently expressed as $I = EQE \times \lambda \times P_{in}/(N \times 1239.85)$, where λ is the wavelength of the optical input in units of nm, P_{in} is the optical power in Watts, and EQE is the OPC's external quantum efficiency. As mentioned previously, since the OPC's resistive losses are proportional to I^2R_{series}, the short wavelengths can be viewed to be advantageous for reducing the resistive power losses.

Furthermore, it has been found that the bandgap voltage offset (W_{oc}) is somewhat constant for semiconductors with different bandgaps.[61] Since W_{oc} directly offsets V_{mpp} from the material bandgap value, it has a larger relative impact on the OPC's efficiency for longer wavelength materials (i.e., smaller bandgaps). For example, assuming a fixed $W_{oc} = 0.25$ eV, a typical value for the OPC's fill factor (e.g., FF ∼ 85%), a typical value for the offset between the input wavelength vs band-edge wavelength (e.g., 65 nm), and all other parameters being comparable, it can be estimated that a 638 nm OPC should have an efficiency about 1.3%abs higher than an OPC at 808 nm. Similarly, an OPC at 1550 nm would have an efficiency 9.3%abs lower than an OPC at 808 nm.

However, it is generally more difficult to obtain the higher bandgap materials with high doping levels and/or high carrier mobility. It is therefore more challenging to support the high sheet conductivity necessary to obtain efficient photocarrier extraction in higher bandgap materials. Consequently, many of the potential benefits of the shorter bandgap materials may be offset by additional resistive losses.

Making high peak current and optically transparent tunnel junctions from higher bandgap material can also be a major challenge. Therefore, the wavelength selection from the viewpoint of the OPC performance is sometimes prescribed by material and technology considerations instead of fundamental considerations.

The multijunction VEHSA strategy has been proven very effective at reducing the operational current in OPCs, by increasing the operating voltage. This voltage/current trade-off makes longer wavelength OPCs manageable, by offsetting the additional resistive losses that would normally occur in single-junction devices.

As an example of shorter wavelength OPCs, Fig. 13 shows the performance of InGaP single-junction devices for optical input powers between 100 and 500 mW. A good efficiency of 59.7% is obtained at the lower input powers and up to 415 mW of output

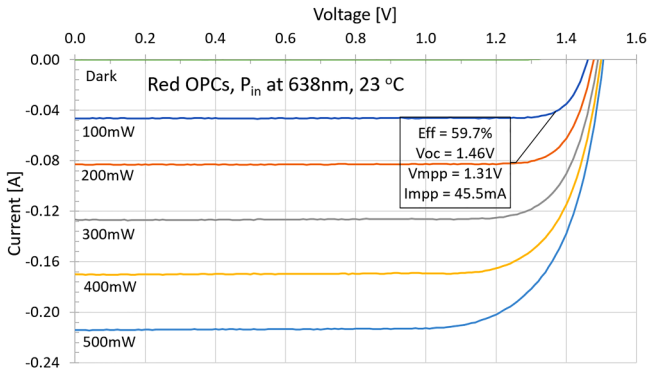

FIG. 13. Measured I–V properties for single-junction InGaP OPC for operation in the red at 638 nm. At 100 mW of input power, an efficiency of Eff = 59.7% is obtained with a V_{oc} of 1.46 V. The output power (P_{mpp}) reaches 242 mW at 500 mW of input power and 415 mW at 1 W (not shown).

power is obtained at an input power of 1 W (not shown). As is the case for most single-junction devices, the efficiency reduction at higher input powers is mainly caused by internal resistive losses. We expect that device optimization and/or a multijunction implementation could significantly improve the InGaP OPC's performance.

For longer wavelength OPCs, we designed and fabricated prototypes of single-junction InGaAs devices for the spectral range of 1500–1600 nm. The devices have been measured to have a record electrical output power levels in excess of 0.5 W. A conversion efficiency of Eff ~ 36% was measured at 1550 nm with an optimal load of ~0.3 Ω.[37]

We expect that devices based on the multijunction InGaAs VEHSA design would exhibit significantly improved operating characteristics and would be of prime interest for some OWPT applications. The ~1550 nm spectral range is particularly important for long-haul fiber tele-communication applications. It is clear that further developments in this area are of interest and we hope soon to be able to report new progresses in this area.

E. Perspective on higher efficiencies

As mentioned in point 3 in Sec. III A, the OPC's conversion efficiency must be maintained high. This is because the impact of the OPC efficiency is leveraged directly in the overall OWPT system and also because it reduces the burden on the system's thermal management.

Continued improvements of the OPC's efficiency in practical applications will require further perfecting the vertical multijunction VEHSA devices. As the OWPT deployments continue to grow, incremental improvements will be obtained simply by exercising the materials and manufacturing processes. Other improvements can be obtained by adjusting the design. For example, this can be achieved by obtaining more precise optical and material constants for the various semiconductor layers. Careful device modeling and quantifying more accurately the impact of photon coupling and recycling in the different subcells can also lead to some improvements.[75]

Higher OPC efficiencies are also achievable by minimizing the thermalization losses caused by the energy difference between the input photons and the bandgap of the absorber. For example, the equivalent of the PT6 of Fig. 7(a) would have an efficiency of 70% simply by reducing the wavelength difference to 14 nm between the bandgap edge and the optical input, while keeping the other parameters at their present measured values of W_{oc} = 0.181 eV and FF = 85.2%.

Incorporating back reflectors[8] is also an interesting device improvement that could readily be incorporated in the VEHSA design.[56]

IV. CONCLUSION

In this paper, we completed a brief overview of the OWPT field from the power converter device perspective. A power converter performance chart has been assembled from the laser power converter results reported in the literature. The study has been performed from the viewpoint of enabling more probe, sensor, or electronic subsystem power capabilities.

We provided perspectives for obtaining stable and reliable power-over-fiber or power beaming devices using vertical multijunction power converters. The devices can be used for remote and galvanically isolated power deployments.

Our study highlights that the roadmap for the future growth will be guided by certain key aspects. The wavelength of operation must be selected to piggyback on developments and advances made in other laser application sectors. These other industries have already achieved laser diode products with high output powers, low $/W, high reliability, and good beam quality. Such optical sources will play a key role in future OWPT deployments. We expect 808 nm to remain in an important spectral range, but ~980 nm to gain significant commercial traction now that more OPC options are available in that spectral range.

New OWPT applications will emerge from the recent availability of higher OPC output powers. Applications that were not possible in the past, due to the lower output power of OPC, will now become reality. To achieve such higher OPC output powers while maintaining high efficiencies, it is necessary to increase the device output voltage. We have highlighted that the higher output powers are in practice only realized using vertical multijunction OPC devices. We have discussed that the OPC's conversion efficiency must be maintained high because the impact of the OPC efficiency is leveraged directly in the overall OWPT system. The higher OPC efficiencies also reduce the burden on the thermal management.

The Perspective, therefore, provides a roadmap for devices achieving not only higher conversion efficiency, but also elaborates on the practical aspects necessary to push the devices to higher output powers. We presented record efficiencies obtained at unprecedented output power capabilities. Output capabilities of 22 W were demonstrated with monolithic discrete devices based on the multijunction VEHSA design. We also demonstrated a 3 × 4 array giving an output power of 44.9 W with a peak efficiency of Eff = 61.6% using Broadcom's AFBR-POC306A1.

The vertical multijunction VEHSA strategy has been proven very effective at reducing the operational current in OPCs. Therefore, the increased current of the longer wavelength OPCs can be managed, which can offset the additional resistive losses that occur normally in single-junction devices. The strategy is expected to extend to new wavelengths in the future. Overall, the high-efficiency vertical multijunction designs enable practical optimal loads and tailored output voltages.

DATA AVAILABILITY

The data that support the findings of this study are available from the corresponding author upon reasonable request.

REFERENCES

[1]R. Jomen, F. Tanaka, T. Akiba, M. Ikeda, K. Kiryu, M. Matsushita, H. Maenaka, P. Dai, S. Lu, and S. Uchida, "Conversion efficiencies of single-junction III–V solar cells based on InGaP, GaAs, InGaAsP, and InGaAs for laser wireless power transmission," Jpn. J. Appl. Phys. **57**, 08RD12 (2018).

[2]Y. Komuro, S. Honda, K. Kurooka, R. Warigaya, F. Tanaka, and S. Uchida, "A 43.0% efficient GaInP photonic power converter with a distributed Bragg reflector under high-power 638 nm laser irradiation of 17 W cm^{-2}," Appl. Phys. Express **14**(5), 052002 (2021).

[3]J. Schubert, E. Oliva, F. Dimroth, W. Guter, R. Loeckenhoff, and A. W. Bett, "High-voltage GaAs photovoltaic laser power converters," IEEE Trans. Electron Devices **56**(2), 170–175 (2009).

[4]Y. Zhao, Y. Sun, Y. He, S. Yu, and J. Dong, "Design and fabrication of six-volt vertically-stacked GaAs photovoltaic power converter," Sci. Rep. **6**, 38044 (2016).

[5]Y.-R. Sun, J.-R. Dong, Y. He, Y.-M. Zhao, S.-Z. Yu, J.-P. Xue, C. Xue, J. Wang, Y. Q. Lu, and Y.-W. Ding, "A six-junction GaAs laser power converter with different sizes of active aperture," Optoelectron. Lett. **13**(1), 21–24 (2017).

[6]J. Yin, J. Yin, Y. Sun, S. Yu, Y. Zhao, R. Li, and J. Dong, "1064 nm InGaAsP multi-junction laser power converters," J. Semicond. **41**(6), 062303 (2020).

[7]J. Huang, Y. Sun, Y. Zhao, S. Yu, J. Dong, J. Xue, C. Xue, C. Xue, J. Wang, Y. Lu, and Y. Ding, "Four-junction AlGaAs/GaAs laser power converter," J. Semicond. **39**(4), 044003 (2018).

[8]H. Helmers, E. Lopez, O. Höhn, D. Lackner, J. Schön, M. Schauerte, M. Schachtner, F. Dimroth, and A. W. Bett, "68.9% efficient GaAs-based photonic power conversion enabled by photon recycling and optical resonance," Phys. Status Solidi RRL **15**, 2100113 (2021).

[9]E. Oliva, F. Dimroth, and A. W. Bett, "Gaas converters for high power densities of laser illumination," Prog. Photovoltaics **16**(4), 289–295 (2008).

[10]J. Mukherjee, S. Jarvis, M. Perren, and S. J. Sweeney, "Efficiency limits of laser power converters for optical power transfer applications," J. Phys. D: Appl. Phys. **46**(26), 264006 (2013).

[11]S. Fafard, M. C. A. York, F. Proulx, C. E. Valdivia, M. M. Wilkins, R. Arès, V. Aimez, K. Hinzer, and D. P. Masson, "Ultrahigh efficiencies in vertical epitaxial heterostructure architectures," Appl. Phys. Lett. **108**, 071101 (2016).

[12]S. Fafard, F. Proulx, M. C. A. York, L. S. Richard, P. O. Provost, R. Arès, V. Aimez, and D. P. Masson, "High-photovoltage GaAs vertical epitaxial monolithic heterostructures with 20 thin p/n junctions and a conversion efficiency of 60%," Appl. Phys. Lett. **109**, 131107 (2016).

[13]V. P. Khvostikov, N. A. Kalyuzhnyy, S. A. Mintairov, S. V. Sorokina, N. S. Potapovich, V. M. Emelyanov, N. K. Timoshina, and V. M. Andreev, "Photovoltaic laser-power converter based on AlGaAs/GaAs heterostructures," Semiconductors **50**(9), 1220–1224 (2016).

[14]L. C. Olsen, D. A. Huber, G. Dunham, and F. W. Addis, "High efficiency monochromatic GaAs solar cells," in *Conference Record of the IEEE Photovoltaic Specialists Conference* (IEEE, 1992), Vol. 1, pp. 419–424.

[15]U. D. Krut, R. Sudharsanan, T. Isshiki, R. King, and N. H. Karam, "A 53% high efficiency GaAs vertically integrated multi-junction laser power converter," in *65th DRC Device Research Conference* (IEEE, 2007), pp. 123–124.

[16]V. Andreev, V. Khvostikov, V. Kalinovsky, V. Lantratov, V. Grilikhes, V. Rumyantsev, M. Shvarts, V. Fokanov, and A. Pavlov, "High current density GaAs and GaSb photovoltaic cells for laser power beaming," in *3rd World Conference on Photovoltaic Energy Conversion, 2003* (IEEE, 2003), pp. 761–764.

[17]R. Peña, C. Algora, and I. Anton, "GaAs multiple photovoltaic converters with an efficiency of 45% for monochromatic illumination," in *Proceedings of the 3rd World Conference on Photovoltaic Energy Conversion* (IEEE, 2003), pp. 228–231.

[18]N. A. Kalyuzhnyy, V. M. Emelyanov, S. A. Mintairov, and M. Z. Shvarts, AIP Conf. Proc. **2012**, 110002 (2018).

[19]Y. Kim, H.-B. Shin, W.-H. Lee, S. H. Jung, C. Z. Kim, H. Kim, Y. T. Lee, and H. K. Kang, "1080 nm InGaAs laser power converters grown by MOCVD using InAlGaAs metamorphic buffer layers," Sol. Energy Mater. Sol. Cells **200**, 109984 (2019).

[20]H. D. Law, W. W. Ng, K. Nakano, P. D. Dapkus, and D. R. Stone, "High efficiency InGaAsP photovoltaic power converter," IEEE Electron Device Lett. **2**(2), 26–27 (1981).

[21]A. N. Panchak, P. V. Pokrovskiy, D. A. Malevskiy, V. R. Larionov, and M. Z. Shvarts, "High-efficiency conversion of high-power-density laser radiation," Tech. Phys. Lett. **45**(1), 24–26 (2019).

[22]A. W. Bett, F. Dimroth, R. Lockenhoff, E. Oliva, and J. Schubert, "III-V solar cells under monochromatic illumination," in *Conference Record of the IEEE Photovoltaic Specialists Conference* (IEEE, 2008), pp. 1–5.

[23]A. L. Fahrenbruch, A. Lopez-Otero, J. G. Werthen, and T. C. Wu, "GaAs- and InAlGaAs-based concentrator-type cells for conversion of power transmitted by optical fibers," in *Conference Record of the IEEE Photovoltaic Specialists Conference* (IEEE, 1996), pp. 117-120.

[24]A. Fave, A. Kaminski, M. Gavand, L. Mayet, and A. Laugier, "GaAs converter for high power laser diode," in *Conference Record of the IEEE Photovoltaic Specialists Conference* (IEEE, 1996), pp. 101–104.

[25]M. A. Green, J. Zhao, A. Wang, and S. R. Wenham, "45% efficient silicon photovoltaic cell under monochromatic light," IEEE Electron Device Lett. **13**(6), 317–318 (1992).

[26]O. Höhn, A. W. Walker, A. W. Bett, and H. Helmers, "Optimal laser wavelength for efficient laser power converter operation over temperature," Appl. Phys. Lett. **108**(24), 241104 (2016).

[27]T. Shan and X. Qi, "Design and optimization of GaAs photovoltaic converter for laser power beaming," Infrared Phys. Technol. **71**, 144–150 (2015).

[28]V. P. Khvostikov, S. V. Sorokina, N. S. Potapovich, O. A. Khvostikova, N. K. Timoshina, and M. Z. Shvarts, "Modification of photovoltaic laser-power ($\lambda = 808$ nm) converters grown by LPE," Semiconductors **52**(3), 366–370 (2018).

[29]V. P. Khvostikov, S. V. Sorokina, N. S. Potapovich, O. A. Khvostikova, and N. K. Timoshina, "Laser ($\lambda = 809$ nm) power converter based on GaAs," Semiconductors **51**(5), 645–648 (2017).

[30]H. Helmers, A. Franke, D. Lackner, O. Höhn, F. Predan, and F. Dimroth, "51% Efficient photonic power converters for O-band wavelengths around 1310 nm," in *Conference Record of the IEEE Photovoltaic Specialists Conference 2020, June* (IEEE, 2020), pp. 2471–2474.

[31]Y. Zhao, P. Liang, H. Ren, and P. Han, "Enhanced efficiency in 808 nm GaAs laser power converters via gradient doping," AIP Adv. **9**(10), 105206 (2019).

[32]M. C. A. York and S. Fafard, "High efficiency phototransducers based on a novel vertical epitaxial heterostructure architecture (VEHSA) with thin p/n junctions," J. Phys. D: Appl. Phys. **50**(17), 173003 (2017).

[33]J. Huang, Y. Sun, Y. Zhao, S. Yu, K. Li, J. Dong, J. Xue, C. Xue, and Y. Ye, "Characterizations of high-voltage vertically-stacked GaAs laser power converter," J. Semicond. **39**(9), 094006 (2018).

[34]Y. Ding, Q. Li, Y. Lu, and J. Wang, "TO-packaged, multi-junction GaAs laser power converter with output electric power over 1W," in *Conference on Lasers and Electro-Optics Pacific Rim (CLEO-PR)* (IEEE, 2017), pp. 1–3.

[35]S. D. Jarvis, J. Mukherjee, M. Perren, and S. J. Sweeney, "Development and characterisation of laser power converters for optical power transfer applications," IET Optoelectron. **8**(2), 64–70 (2014).
[36]V. P. Khvostikov, S. V. Sorokina, O. A. Khvostikova, N. S. Potapovich, A. V. Malevskaya, M. V. Nakhimovich, and M. Z. Shvarts, AIP Conf. Proc. **2149**, 050007 (2019).
[37]S. Fafard, D. Masson, J.-G. Werthen, J. Liu, T. C. Wu, C. Hundsberger, M. Schwarzfischer, G. Steinle, C. Gaertner, C. Piemonte, B. Luecke, J. Wittl, and M. Weigert, "Power and spectral range characteristics for optical power converters," Energies **14**(15), 4395 (2021).
[38]G. Keller, "GaAs multi-junction laser power converters at AZUR SPACE: Current status and development activities," in *1st Optical Wireless and Fiber Power Transmission Conference, Yokohama, Japan* (2019).
[39]S. J. Wojtczuk, "Long-wavelength laser power converters for optical fibers," in *Conference Record of the Twenty Sixth IEEE Photovoltaic Specialists Conference - 1997* (IEEE, 1997), pp. 971–974.
[40]N. Eggert, R. Rusack, and J. Mans, "Evaluation of photonic power converters," J. Instrum. **5**, T02001 (2010).
[41]S. Fafard and D. Masson, this study: [41a] is Fig. 13 for InGaP 1J, [41b] is Fig. 8 for PT12-808 nm, [41c] is PT5 at $P_{in} = 25$ W at 811 nm with measured $V_{mpp} = 5.55$ V and $I_{mpp} = 2.482$ A, and [41d] is PT6 at $P_{in} = 28.4$ W at 811 nm measured at $R_{load} = 2.46$ Ohms with V = 6.57 V and I = 2.67 A (2021).
[42]A. W. Bett, F. Dimroth, R. Lockenhoff, E. Oliva, and J. Schubert, "III–V solar cells under monochromatic illumination," in *2008 33rd IEEE Photovoltaic Specialists Conference, 2008* (IEEE, 2008), pp. 1–5.
[43]M. Matsuura, H. Nomoto, H. Mamiya, T. Higuchi, D. Masson, and S. Fafard, "Over 40-W electric power and optical data transmission using an optical fiber," IEEE Trans. Power Electron. **36**(4), 4532 (2020).
[44]H. Helmers, C. Armbruster, M. von Ravenstein, D. Derix, and C. Schöner, "6-W optical power link with integrated optical data transmission," IEEE Trans. Power Electron. **35**, 7904 (2020).
[45]P. Jaffe, P. Jenkins, T. Nugent *et al.*, see https://youtu.be/Xb9THqrXd4I for (US NRL), PowerLight Tech. Inc. (2019).
[46]M. Wilkins, M. Ishigaki, P.-O. Provost, D. Masson, S. Fafard, C. E. Valdivia, E. M. Dede, and K. Hinzer, "Ripple-free boost-mode power supply using photonic power conversion," IEEE Trans. Power Electron. **34**, 1054 (2018).
[47]S. Fafard, M. C. A. York, F. Proulx, M. Wilkins, C. E. Valdivia, M. Bajcsy, D. Ban, R. Arès, V. Aimez, K. Hinzer, M. Ishigaki, and D. P. Masson, "Ultra-efficient N-junction photovoltaic cells with $V_{oc} > 14$ V at high optical input powers," in *PVSC 2016—IEEE 43rd Photovoltaic Specialists Conference* (IEEE, 2016), p. 2374.
[48]R. M. France, J. Buencuerpo, M. Bradsby, J. F. Geisz, Y. Sun, P. Dhingra, M. L. Lee, and M. A. Steiner, "Graded buffer Bragg reflectors with high reflectivity and transparency for metamorphic optoelectronics," J. Appl. Phys. **129**, 173102 (2021).
[49]M. N. Beattie, C. E. Valdivia, M. M. Wilkins, M. Zamiri, K. L. C. Kaller, M. C. Tam, H. S. Kim, J. J. Krich, Z. R. Wasilewski, and K. Hinzer, "High current density tunnel diodes for multi-junction photovoltaic devices on InP substrates," Appl. Phys. Lett. **118**, 062101 (2021).
[50]L. Wagner, S. K. Reichmuth, S. P. Philipps, E. Oliva, A. W. Bett, and H. Helmers, "Integrated series/parallel connection for photo-voltaic laser power converters with optimized current matching," Prog. Photovoltaics: Res. Appl. **29**, 172 (2020).
[51]A. Panchak, V. Khvostikov, and P. Pokrovskiy, "AlGaAs gradient waveguides for vertical p/n junction GaAs laser power converters," Opt. Laser Technol. **136**, 106735 (2021).
[52]M. Lin, W. E. I. Sha, W. Zhong, and D. Xu, "Intrinsic losses in photovoltaic laser power converters," Appl. Phys. Lett. **118**, 104103 (2021).
[53]Y. Zhao, S. Li, H. Ren, S. Li, and P. Han, "Energy band adjustment of 808 nm GaAs laser power converters via gradient doping," J. Semicond. **42**, 032701 (2021).
[54]N. Nouri, C. E. Valdivia, M. N. Beattie, M. S. Zamiri, J. J. Krich, and K. Hinzer, Proc. SPIE **11681**, 116810X (2021).
[55]D. Masson, F. Proulx, and S. Fafard, "Pushing the limits of concentrated photovoltaic solar cell tunnel junctions in novel high-efficiency GaAs photo-transducers based on a vertical epitaxial heterostructure architecture," Prog. Photovoltaics **23**, 1687 (2015).
[56]S. Fafard and D. P. Masson, "Transducer to convert optical energy to electrical energy," US patent 9,673,343 (June 6, 2017).
[57]J. Wulf, E. Oliva, G. Mikolasch, J. Bartsch, F. Dimroth, and H. Helmers, "Thin film GaAs solar cell enabled by direct rear side plating and patterned epitaxial lift-off," in *2021 IEEE 48th Photovoltaic Specialists Conference (PVSC), 2021* (IEEE, 2021), pp. 1931–1935.
[58]H. Helmers *et al.*, "Pushing the boundaries of photovoltaic light to electricity conversion: A GaAs based photonic power converter with 68.9% efficiency," in *2021 IEEE 48th Photovoltaic Specialists Conference (PVSC)* (IEEE, 2021), pp. 2286–2289; M. Schauerte, O. Höhn, T. Wierzkowski, G. Keller, and H. Helmers, "4-junction GaAs based thin film photonic power converter with back surface reflector for medical applications," in *2021 IEEE 48th Photovoltaic Specialists Conference (PVSC)* (IEEE, 2021), pp. 1954–1959.
[59]R. M. France *et al.*, "Improvement of front-junction GaInP by point-defect injection and annealing," in *2021 IEEE 48th Photovoltaic Specialists Conference (PVSC)* (IEEE, 2021), pp. 2522–2524.
[60]J. F. Geisz, J. Buencuerpo, W. E. McMahon, T. R. Klein, A. C. Tamboli, and E. L. Warren, "Fabrication, measurement, and modeling of GaInP/GaAs three-terminal cells and strings," in *2021 IEEE 48th Photovoltaic Specialists Conference (PVSC)*, (IEEE, 2021), pp. 0154–0157.
[61]M. Yamaguchi, F. Dimroth, J. F. Geisz, and N. J. Ekins-Daukes, "Multi-junction solar cells paving the way for super high-efficiency," J. Appl. Phys. **129**, 240901 (2021).
[62]F. Proulx, M. C. A. York, P. O. Provost, R. Arès, V. Aimez, D. P. Masson, and S. Fafard, "Measurement of strong photon recycling in ultra-thin GaAs n/p junctions monolithically integrated in high-photovoltage vertical epitaxial heterostructure architectures with conversion efficiencies exceeding 60%," Phys. Status Solidi RRL **11**, 1600385 (2017).
[63]M. Wilkins, C. E. Valdivia, A. M. Gabr, D. Masson, S. Fafard, and K. Hinzer, "Luminescent coupling in planar opto-electronic devices," J. Appl. Phys. **118**, 143102 (2015).
[64]E. Lopez, O. Höhn, M. Schauerte, D. Lackner, M. Schachtner, S. K. Reichmuth, and H. Helmers, "Experimental coupling process efficiency and benefits of back surface reflectors in photovoltaic multi-junction photonic power converters," Prog. Photovoltaics. **29**, 461 (2021).
[65]D. Xia and J. J. Krich, "Efficiency increase in multijunction monochromatic photovoltaic devices due to luminescent coupling," J. Appl. Phys. **128**, 013101 (2020).
[66]Y. Yamagata, Y. Yamada, Y. Kaifuchi, R. Nogawa, R. Morohashi, and M. Yamaguchi, "Performance and reliability of high power, high brightness 8xx-9xx nm semiconductor laser diodes," in *Proceedings of the 2015 IEEE High Power Diode Lasers and Systems Conference (HPD), Coventry, UK, 14–15 October 2015* (IEEE, 2015), pp. 7–8.
[67]R. Kimovec, H. Helmers, A. W. Bett, and M. Topič, "Comprehensive electrical loss analysis of monolithic interconnected multi-segment laser power converters," Prog. Photovoltaics **27**, 199 (2019).
[68]R. Kimovec, H. Helmers, A. W. Bett, and M. Topič, "On the influence of the photo-induced leakage current in monolithically interconnected modules," IEEE J. Photovoltaics **8**, 541–546 (2018).
[69]N. A. Kalyuzhnyy, V. M. Emelyanov, V. V. Evstropov, S. A. Mintairov, M. A. Mintairov, M. V. Nahimovich, R. A. Salii, and M. Z. Shvarts, "Optimization of photoelectric parameters of InGaAs metamorphic laser (λ=1064 nm) power converters with over 50% efficiency," Sol. Energy Mater. Sol. Cells **217**, 110710 (2020).
[70]T. He, S.-H. Yang, H.-Y. Zhang, C.-M. Zhao, Y.-C. Zhang, P. Xu, and M. A. Muñoz, "High-power high-efficiency laser power transmission at 100 m using optimized multi-cell GaAs converter," Chin. Phys. Lett. **31**(10), 104203 (2014).

[71]V. P. Khvostikov, N. A. Kalyuzhnyy, S. A. Mintairov, N. S. Potapovich, S. V. Sorokina, and M. Z. Shvarts, "Module of laser-radiation (λ = 1064 nm) photovoltaic converters," Semiconductors **53**(8), 1110–1113 (2019).
[72]L. Li, H.-M. Ji, S. Luo, P. Xu, Q. Gao, H. Lv, and W. Liu, "Fabrication and characterization of a high-power assembly with a 20-junction monolithically stacked laser power converter," IEEE J. Photovoltaics **8**(5), 1355–1362 (2018).
[73]E. F. Fernández, F. Almonacid, P. Rodrigo, and P. Pérez-Higueras, "Calculation of the cell temperature of a high concentrator photovoltaic (HCPV) module: A study and comparison of different methods," Sol. Energy Mater. Sol. Cells **121**, 144–151 (2014).
[74]S. J. Sweeney, "Optical wireless power at eye-safe wavelengths: Challenges and opportunities," in *3rd Optical Wireless and Fiber Power Transmission Conference (OWPT2021), Yokohama, Japan, 19–22 April 2021* (2021).
[75]S. Čičić and S. Tomić, "Automated design of multi junction solar cells by genetic approach: Reaching the >50% efficiency target," Sol. Energy Mater. Sol. Cells **181**, 30–37 (2018).